Refraction-aware integrated Georeferencing of bathymetric Laser Scanning Data

Gottfried Mandlburger[1,*], Lucas Dammert[1], Jan Rhomberg-Kauert[1], Florian Pöppl [2], Martin Pfennigbauer[2]

[1] TU Wien, Department of Geodesy and Geoinformation, 1040 Vienna, Austria
(gottfried.mandlburger, lucas.dammert, jan.rhomberg-kauert)@geo.tuwien.ac.at
[2] *RIEGL* Laser Measurement Systems GmbH, 3580 Horn, Austria – (fpoeppl, mpfennigbauer)@riegl.com

Keywords: Topo-bathymetric LiDAR, Refraction correction, Strip adjustment, Trajectory estimation

Abstract

Bathymetric Laser Scanning (BLS) enables high-resolution mapping of underwater topography using green-wavelength laser pulses that penetrate the water column. However, precise georeferencing of the BLS data is affected by refraction at the air–water interface, which displaces submerged features and affects conventional strip adjustment methods. This paper introduces an integrated refraction-aware georeferencing workflow that combines refraction correction with trajectory and boresight optimization within a unified adjustment framework. Implemented using the scientific OPALS laser scanning software, the workflow starts with direct georeferencing of uncorrected laser returns, derives a water surface model, applies Snell's law-based refraction correction, and performs iterative strip adjustment until convergence. The approach was validated using UAV-borne topo-bathymetric LiDAR data from Lake Alm (Almsee) in Upper Austria, captured with a *RIEGL* VQ-840-GE sensor system. Comparative analysis across multiple processing scenarios demonstrates that the proposed integrated method significantly improves internal consistency between overlapping flight strips. The residual height discrepancies, quantified by the median absolute deviation (σ_{MAD}), were reduced from $4.5\,\mathrm{cm}$ using standard processing workflows to $2.1\,\mathrm{cm}$ with the integrated approach — an improvement exceeding 50%. A single processing pass was sufficient for the relatively calm conditions of the test site, though iterative refinement may benefit more dynamic water surfaces. The presented methodology is generic and can be embedded in any laser scanning framework supporting modular georeferencing and refraction correction.

1. Introduction

Bathymetric Laser Scanning (BLS) is an active multi-sensor measurement technique to capture 3D underwater topography using pulsed lasers operating in the green domain of the visible spectrum, typically $532\,\mathrm{nm}$ (Guenther et al., 2000). The emitted laser pulses travel through the atmosphere, partially reflect at the air-water interface, further propagate into the water column, and reflect a second time at the bottom of the water body or even multiple times if objects like vegetation are in the laser line of sight. At the water surface, the laser beam is deflected according to Snell's law of refraction and propagates with reduced velocity in water. Thus, refraction and runtime correction is a core component in the BLS processing chain.

The technology itself dates back to the 1960s, when it was first used in the military sector (Hickman and Hogg, 1969), followed by civil applications for near-shore nautical charting (Guenther, 1985) and coastal mapping (Wozencraft and Lillycrop, 2003). Around 2010, a new generation of topo-bathymetric LiDAR (Light Detection and Ranging) designed for simultaneous acquisition of topography and bathymetry was introduced (Fuchs and Tuell, 2010), and the application fields extended from the maritime area to inland waters (Pfennigbauer et al., 2011). Recently, sensor miniaturization and advances in carrier platform technology enabled the integration of relatively light weight bathymetry laser scanners onto Remotely Piloted Aerial Systems (RPAS), also called Uncrewed Aerial Vehicle (UAV) or drones (Kinzel and Legleiter, 2019; Mandlburger et al., 2020). Regardless of the size and weight of the carrier platform and sensor, the BLS is always operated from the air, and data is collected along regular flight routes to ensure comprehensive coverage of the bathymetry in shallow waters. For processing BLS data, this poses the challenge of dealing with both sensor orientation and laser ray refraction simultaneously.

Refraction correction of the raw bathymetric LiDAR observations is based on a digital representation of the continuous water surface. In case of still water surfaces like ponds and small- to medium-sized lakes, the water surface can be modeled with simple geometric primitives like horizontal or slightly tilted planes and can therefore be derived from auxiliary observation data (GNSS, total station, leveling device) with sufficient accuracy. For highly dynamic wavy water bodies, such as meandering rivers or wavy coastal areas, the air-water interface must be directly derived from the LiDAR data. To obtain reliable estimates of the instantaneous water surface, topo-bathymetric laser scanners employ a secondary infrared laser in addition to the water-penetrating green laser channel (Guenther et al., 2000) or sophisticated full waveform processing is applied to extract both the surface and the bottom from the complex return signal (Schwarz et al., 2019). If the water surface model is derived directly from the laser data, the extracted water surface returns must be georeferenced.

BLS sensors employ a Global Navigation Satellite System (GNSS) and an Inertial Measurement Unit (IMU) to position and orient the measurement platform. To obtain georeferenced coordinates of the laser returns, the scanner's measurements (range, beam deflection angle) are first transformed to 3D cartesian coordinates in the scanner's own coordinate system and then transformed to Cartesian Earth-Centered-Earth-Fixed (ECEF) coordinates based on the trajectory (i.e., direct georeferencing). Errors of the georeferenced laser points, which can be attributed to inaccuracies in the measurement data (GNSS, IMU, scanner) and the mounting calibration (lever

* Corresponding author

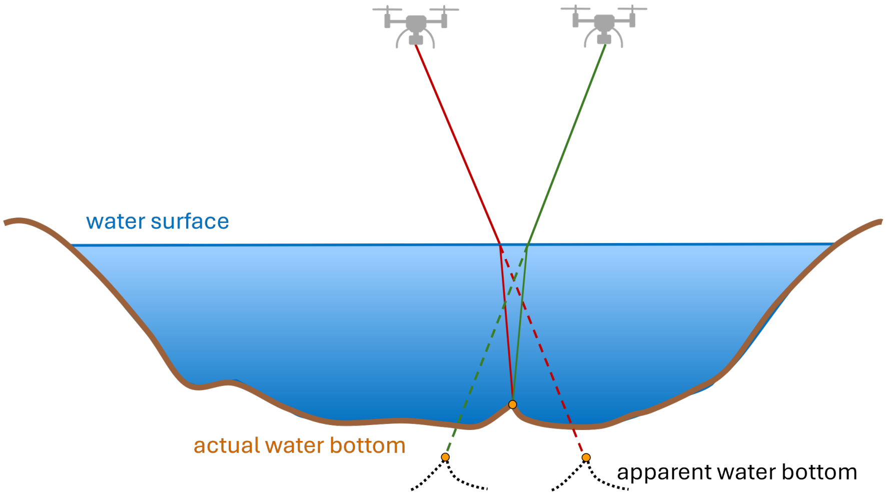

Figure 1. Schematic diagram of displacement of submerged features due to laser ray refraction at the air-water interface.

arms, boresight angles), are typically minimized by strip adjustment.

Various approaches have been presented in the literature for the adjustment of kinematic laser scan data, in particular for the compensation of residual errors of the trajectory and the sensor mounting and calibration. Glira et al. (2015) introduced an Airborne Laser Scanning (ALS) strip adjustment framework based on variants of the Iterative Closest Point (ICP) algorithm (Besl and McKay, 1992). The primary framework was further extended to compensate for time-dependent trajectory errors (Glira et al., 2016) and to integrate concurrently captured images in the adjustment (Jonassen et al., 2023). Brun et al. (2022) proposed a procedure to adjust flight trajectories based on 3D point–to–point correspondences between points of overlapping flight strips within a joint adjustment together with raw inertial and GNSS observations. A similar path of tightly coupling laser and inertial data and loose coupling of laser and GNSS data is introduced in Pöppl et al. (2024).

In all cited articles (Glira et al., 2015, 2016; Brun et al., 2022; Jonassen et al., 2023; Pöppl et al., 2024), corresponding features in overlapping flight lines are used as the basis for compensating or mitigating trajectory errors. The correspondences are established in the object space, i.e., an Earth-Centered-Earth-Fixed (ECEF) cartesian coordinate system. However, in BLS the correspondences are compromised by ray refraction at the air-water interface (Szafarczyk and Toś, 2023) as shown in Figure 1. In general, the coordinate differences of the corresponding features are minimized within the strip adjustment, and the unknown parameters (trajectory errors, boresight misalignment, lever arms, scanner calibration parameters) are estimated to mitigate the coordinate differences. If a large part of the acquired data is over dry land, e.g. for topo-bathymetric surveys of small inland waters such as rivers and ponds, the errors introduced when using uncorrected points are often negligible (Pöppl et al., 2024). However, if the underwater portion predominates, this deteriorates the estimation of the boresight angles, lever arms, and trajectory if refraction is not considered during georeferencing, leading to large discrepancies in the strip overlap area. In this case, refraction correction and strip adjustment must be performed simultaneously or at least coordinated. To the best of our knowledge, this is not described in the related literature so far.

We therefore propose a strategy to embed refraction correction in an integrated georeferencing approach and test the procedure with BLS data acquired at an Alpine lake in Upper Austria (Almsee). We describe the study site and the acquired BLS data in Section 2 and the proposed data processing pipeline in Section 3. In Section 4, we present the results followed by a critical discussion in Section 5. Section 6 concludes the article with a summary and outlook on future work.

2. Materials

To validate the proposed integrated georeferencing strategy, we conducted a UAV flight with a topo-bathymetric laser scanner system at Almsee, Upper Austria, in August 2025. The study site is shown in Figure 2. Almsee is a mountain lake in the Upper Austrian part of the Salzkammergut region. The outflow of Almsee is the Alm River, which drains into the Danube through the Traun River. With its largely natural shores, highly diverse vegetation belt and adjacent wetlands, this nutrient-poor lake provides habitats for many animal and plant species. It represents a relatively intact ecosystem and the area has been a protected nature reserve since 1965. The lake is located at an elevation of 589 m above sea level (ellipsoidal height: 634.5 m). The lake, which stretches from north to south, is 2.3 km long and has a maximum width of 700 m. Its surface area is approximately 85 hectares. The shallow lake exhibits a mean depth of around 3 m and features occasional sinkholes with a maximum depth of 9 m.

The entire lake was captured with a compact *RIEGL* VQ-840-GE airborne LiDAR system for combined topographic and bathymetric surveying (Riegl, 2025). The instrument weighs 10.3 kg including the integrated GNSS/IMU navigation device and was mounted on an Acecore Noa quadcopter UAV with a maximum take-off mass (MTOM) of 36.9 kg (cf. Figure 3). The laser scanner was operated from a flying altitude of 120 m above ground level (agl) with a flight speed of 8 m/s, a pulse repetition rate of 100 kHz and a beam divergence of 1 mrad. This results in a size of the laser footprint at the water surface of 12 cm and a single-strip median point density of 45 points/m^2. In total, the lake was captured with 4 flights and a total air time of 65 min. The entire flight mission consisted of 59 separate flight lines, which were jointly processed with the procedure outlined in the next section.

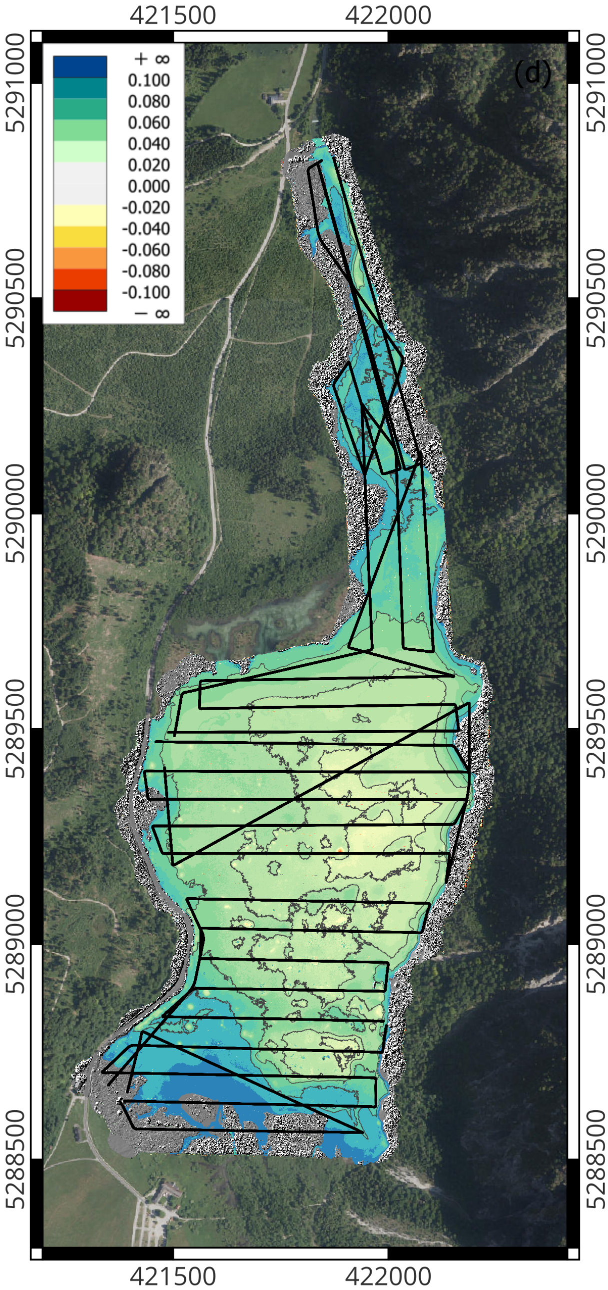

Figure 2. Study area Almsee, Upper Austria. Orthophoto map (basemap.at) superimposed with color coded water depth map and depth isolines. Map coordinate reference system: ETRS89/UTM 33 (EPSG:25833). WGS84 coordinates: $47°45'N, 13°57'E$.

Figure 3. *RIEGL* VQ-840-GE topo-bathymetric laser scanner mounted on an Acecore Noa quadcopter UAV during data acquisition at Almsee in August 2025

3. Methods

Figure 4 shows the general workflow for integrated, refraction-aware georeferencing of BLS data. The processing pipeline consists of the following steps:

1. Initial trajectory estimation based on GNSS and IMU observations, e.g. via Kalman filtering
2. Direct georeferencing of the raw (i.e., uncorrected) laser returns
3. Derivation of a water surface model grid either from auxiliary measurements or from the raw georeferenced BLS point cloud
4. Refraction correction of the georeferenced laser returns
5. Optimization of trajectory and boresight alignment via strip adjustment
6. Error evaluation with focus on residual height discrepancies in overlapping flight areas
7. Repeat steps 3-6 until convergence

The method described is generic and can be integrated into any laser scanning software. In our case, we used the scientific laser scanning software OPALS (Pfeifer et al., 2014), which facilitates the implementation of the workflow due to its purely modular structure. In particular, we used the following OPALS modules (TU Wien, 2026):

- *DirectGeoref*: The module takes a time-stamped 3D laser point cloud stored in scanner coordinates (t, x, y, z), the flight trajectory in georeferenced coordinates (t, easting, northing, elevation, roll, pitch, yaw), and information about the mounting of the scanner system as input and returns the laser point cloud in the georeferenced coordinate system defined by the trajectory, i.e., ETRS89/UTM33 in our case. Note that both the trajectory and the laser points must be time-stamped and synchronized. Typically, GPS time (adjusted GPS time, GPS day seconds, GPS week seconds) is used as the common time system of both data streams. The module output is a data set stored in the OPALS Data Manager (ODM) file format (Otepka et al., 2012).

https://doi.org/10.5194/isprs-archives-XLIX-B2-2026-963-2026 |

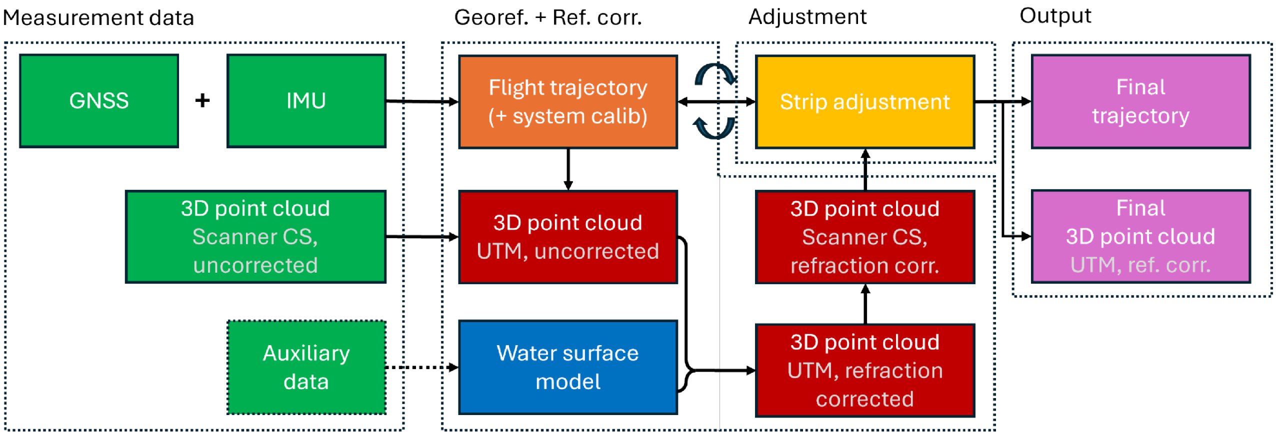

Figure 4. Schematic workflow diagram for integrated, refraction-aware georeferencing of the BLS data.

- *Import*: The general aim of the *Import* module is to transform (georeferenced) 3D point clouds stored in arbitrary data formats into the internal ODM structure. In addition, the module also provides functionality to calculate the laser beam vector, selectable in scanner and/or georeferenced coordinates, by simultaneously reading and analyzing both the trajectory and the laser point cloud. The availability of beam vector information is a prerequisite for (i) strip adjustment and (ii) refraction and runtime correction.

- *Snellius*: This module performs refraction and runtime correction. The basic input is the georeferenced point cloud that includes beam vector information, a water surface model provided as a raster file or constant height, and the refractive index of water. Different refractive indices for the phase velocity of the laser light and the group velocity of the laser pulse are supported (Schwarz et al., 2021). For each point, the module intersects the laser beam with the water surface and corrects the underwater part of the laser ray according to Snell’s law of refraction. The module output is a refraction corrected data set stored in ODM file format.

- *StripAdjust*: This module takes (i) the 3D laser point cloud in scanner coordinates, (ii) the trajectory, (iii) scanner mounting parameters, and (iv) ground control information (points, patches) as input and gives optimized parameters (system calibration, trajectory, georeferenced 3D laser point cloud) as output. The module provides different trajectory correction models (Glira et al., 2016). For our tests, we used a simple bias model, which estimates for each flight strip constant correction terms for each component of the trajectory (easting, northing, height, roll, pitch, yaw).

After running the integrated procedure, we calculated the residual strip differences in a standard quality control step (Ressl et al., 2008). We assessed the performance of the proposed method via σ_{MAD}, a robust estimator of the strip height differences, derived in smooth parts of all overlapping flight strips.

4. Results

We tested the procedure described in Section 3 with the Almsee BLS data set detailed in Section 2. The difference in height from the lake’s source to the outlet is not greater than $15\,\mathrm{cm}$. This allowed us to model the water surface with a horizontal water level of $634.5\,\mathrm{m}$ above the ETRS89 ellipsoid as the first approximation and as a single tilted plane in a repeat pass of the workflow (i.e., 2^{nd} iteration). Figure 5 shows a shaded DEM relief map superimposed with a color-coded map of height differences in smooth parts of overlapping flight strips. In case of a perfectly calibrated system and an error-free trajectory, all strip height differences would be zero (white). In fact, the strip difference maps show height discrepancies that range from less than $-5\,\mathrm{cm}$ (dark red) to more than $5\,\mathrm{cm}$ (dark blue).

In order to quantify the performance of the proposed approach in comparison with standard processing workflows, we tested the following scenarios:

(a) Direct georeferencing + refraction correction: The laser points are directly georeferenced with a Smoothed Best Estimate Trajectory (SBET) and the sensor system’s precalibrated mounting parameters. Refraction and runtime correction is applied based on the resulting georeferenced point clouds but without prior strip adjustment.

(b) Refraction correction after adjustment of uncorrected points: This mimics a standard laser scanning workflow as implemented (trajectory estimation, echo detection, georeferencing and strip adjustment). Strip adjustment is carried out with the uncorrected laser points. Systematic errors due to not considering the refraction effect deteriorate the parameters estimated within the strip adjustment. Only after the adjustment, refraction and runtime correction is performed for the resulting point cloud.

(c) Proposed workflow: single pass: In this scenario a full pass of the proposed workflow (steps 1-7) is performed.

(d) Proposed workflow: two passes: In this case, we performed processing steps 1-5 and then used the optimized trajectory and mounting calibration for a second pass of the workflow (steps 3-5) followed by the final quality control step 6.

Figure 5 demonstrates the performance of the presented approach. Scenario (a) based on direct georeferencing only shows large systematic strip height differences, which can be attributed to restricted GNSS reception in the lake’s narrow valley. Scenario (b) implementing a standard laser data processing

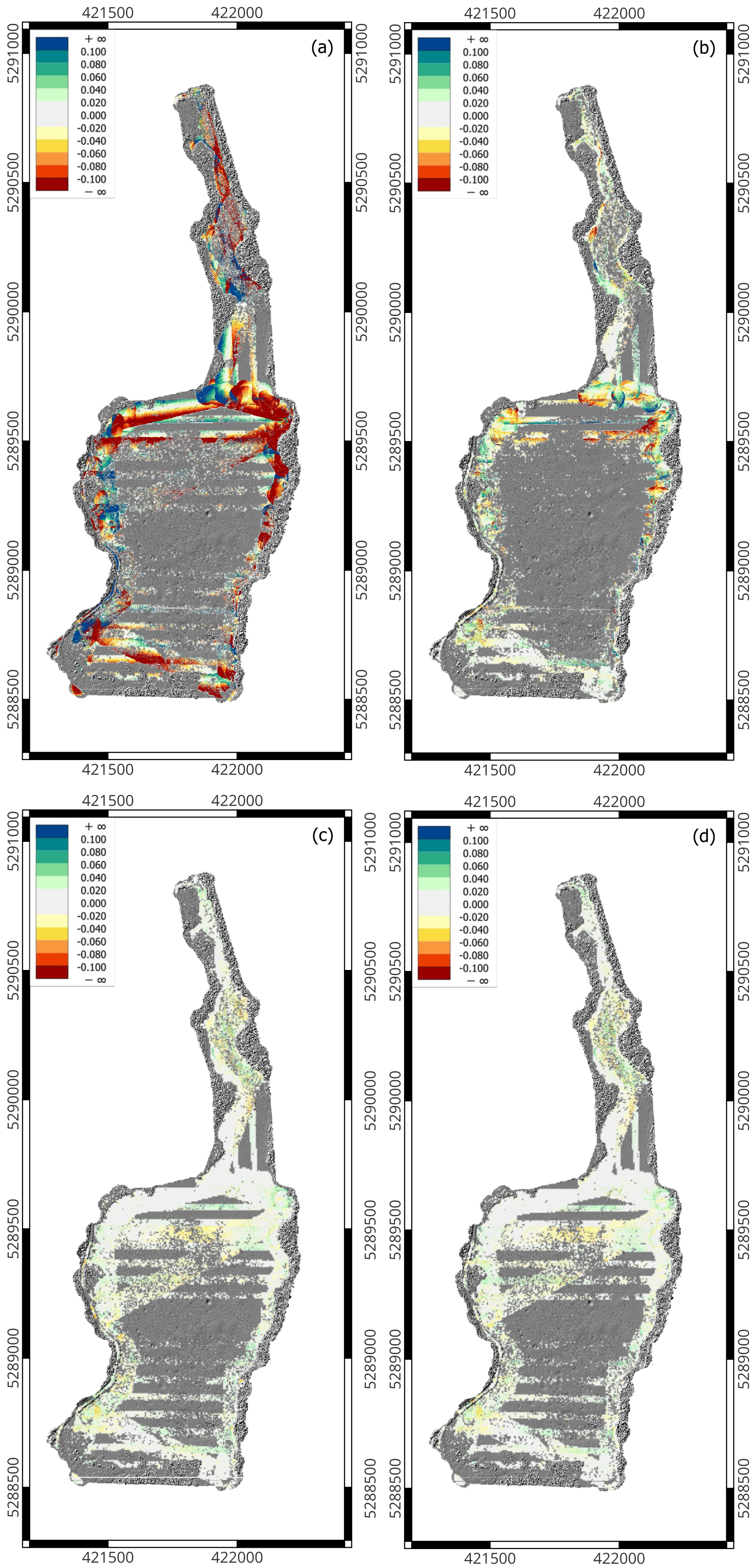

Figure 5. Results of integrated, refraction-aware georeferencing at study area Almsee, Upper Austria. color coded strip height differences (in m) in smooth surface areas; (a) direct georeferencing + refraction correction; (b) strip adjustment of uncorrected points + refraction correction after strip adjustment; (c) proposed workflow, single pass; (d) proposed workflow, double pass.

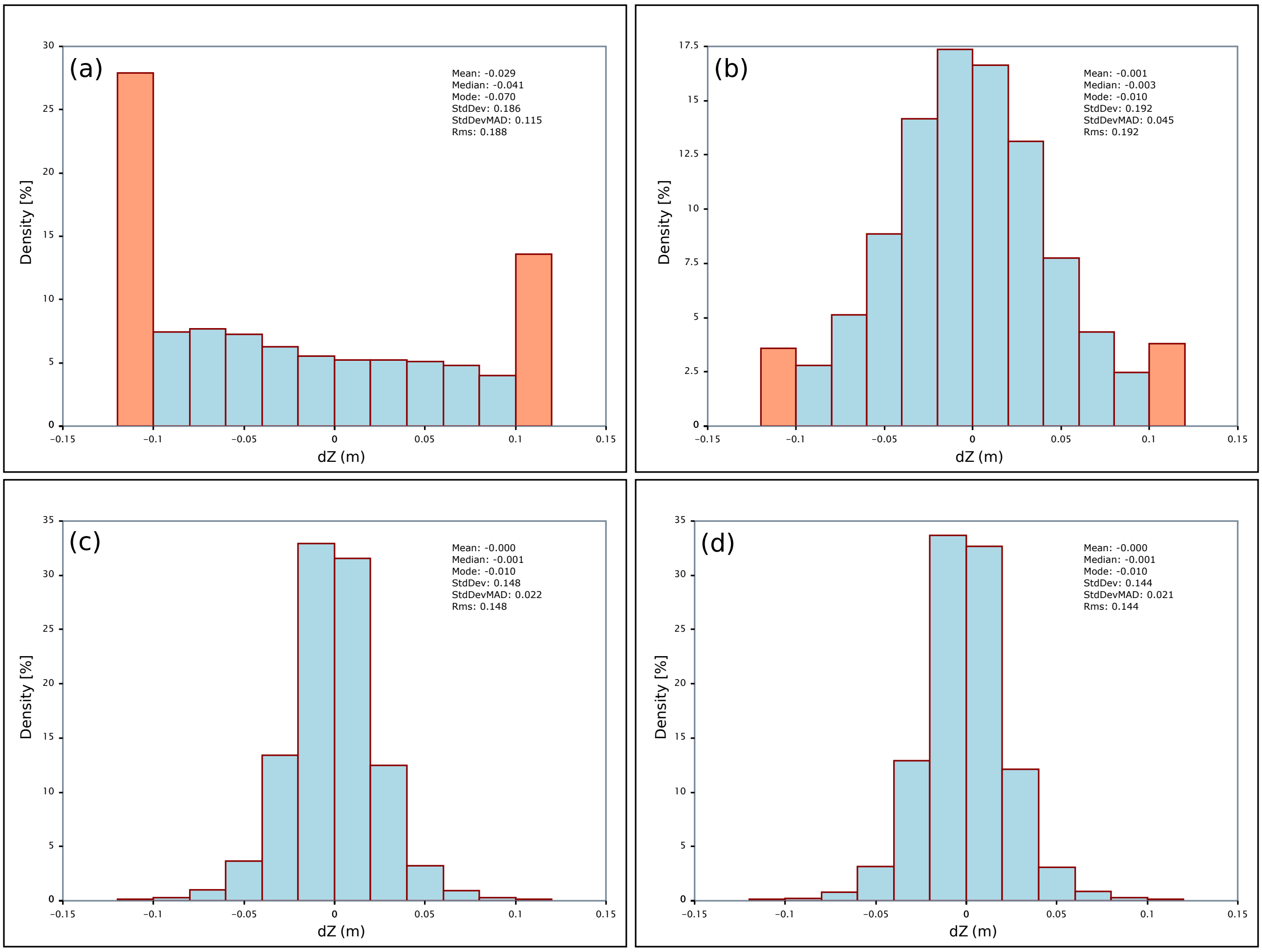

Figure 6. Histograms of the residual strip height differences for the four processing scenarios displayed in Figure 5; (a) direct georeferencing + refraction correction; (b) strip adjustment of uncorrected points + refraction correction after strip adjustment; (c) proposed workflow, single pass; (d) proposed workflow, double pass.

workflow shows lighter, improved results (less saturated colors), but still, remaining systematic deviations persist especially in the deeper parts of the lake where the effect of not considering refraction-induced errors is more pronounced. Using the proposed integrated workflow effectively reduces the residual height discrepancies in overlapping flight lines. This applies to both the single-pass (c) and double-pass (d) execution of the workflow. In both cases, the predominant whitish colors indicate deviations in the cm-range. The 2^{nd} iteration (d) only marginally improves the results.

The strip difference histograms corresponding to the color-coded maps of Figure 5 are plotted in Figure 6. From (a) to (d) the distribution of the height differences gradually gets more centered around zero, with pronounced improvements when running the proposed method (c, d) compared to standard processing (a, b) and with only slight differences between the single-pass (c) and the double-pass (d) execution of the integrated workflow. σ_{MAD} improves from initially $11.5\,\mathrm{cm}$ for (a) and $4.5\,\mathrm{cm}$ for (b) to $2.1\,\mathrm{cm}$ for (c) and (d). Thus, the residual height deviations are reduced to 50% compared to the standard workflow (b).

Table 1 reports in detail the height difference distribution (centiles, deciles, quartiles). All reported metrics gradually improve from (a) to (d). In particular, the interquartile range (IQR: Q75%-Q25%) improves from $4.5\,\mathrm{cm}$ for the standard laser data processing workflow (b) to $2.1\,\mathrm{cm}$ for the proposed integrated workflow (d). The same applies to the interdecile range (IDC: Q90%-Q10%) with an improvement from 9.8 (b) to $4.5\,\mathrm{cm}$ (d).

5. Discussions

The errors in scenario (a) (direct georeferencing) can be attributed to inaccuracies in the trajectory, as the steep topography surrounding the lake entails a suboptimal satellite configuration. The application of a standard BLS data processing workflow (b), which performs refraction and runtime correction only after strip adjustment and georeferencing (b), improves the results compared to (a), but the strip adjustment performs poorly as the corresponding submerged feature do not match properly. The geometric displacement scales with water depth, leading to smaller residual discrepancies in shallow water areas and larger deviations in deeper regions. This can be clearly seen when comparing the water depth map of Figure 2 with the color-coded height differences of Figure 5b. Smaller deviations occur in the southern part of the lake, where the lake is less than $1\,\mathrm{m}$ deep.

Although we proposed an iterative workflow, the second pass did not significantly improve the results. For the second pass, we re-calculated the water surface model and changed from

	Q1%	Q5%	Q10%	Q25%	Q50%	Q75%	Q90%	Q95%	Q99%
(a)	-0.294	-0.184	-0.142	-0.086	-0.024	0.043	0.104	0.144	0.245
(b)	-0.143	-0.073	-0.051	-0.023	-0.001	0.021	0.047	0.071	0.166
(c)	-0.067	-0.035	-0.024	-0.011	-0.000	0.010	0.023	0.034	0.068
(d)	-0.064	-0.033	-0.023	-0.011	-0.000	0.010	0.022	0.033	0.066

Table 1. Quantile statistics of strip height differences for processing scenarios a-d according to Figure 5. Units in (m)

an approximate description with a constant water level derived from averaged RTK-GNSS measurements to an explicit modeling of the water surface based on the laser returns. However, since the lake is almost level in the approximately 2 km range from its source to the outlet with a height difference of less than 15 cm, the effect of an improved water surface model in the second iteration did not have a large impact on the final results. This might change if the fluctuation of the water surface height is large, as is, for example, the case for mountain streams and even lowland rivers. However, for the Almsee data set, a single pass of the proposed integrated workflow was enough.

6. Conclusions

In this article, we introduced an integrated approach for georeferencing bathymetric laser scanning data. The approach starts with direct georeferencing of the raw laser returns based on an SBET trajectory and performs refraction and runtime correcting of the raw 3D point cloud based on a first approximate water surface model. Strip adjustment and fine georeferencing based on control points and patches is then performed with the refraction corrected point clouds, which overcomes potential feature matching problems, when using the uncorrected 3D points as input for strip adjustment. As the first pass uses approximate parameters (trajectory, mounting calibration, water surface model), the entire procedure can be repeated iteratively with gradually improved trajectories, system calibration, and water surface models, till convergence is reached.

The proposed method was evaluated with real-world data from a UAV-borne BLS data acquisition carried out at Almsee, Upper Austria in August 2025. Compared to standard BLS data processing, the residual height discrepancies could be reduced from 4.5 cm to 2.1 cm, which corresponds to an improvement of more than 50%. For the concrete Almsee data set, a single pass of the workflow proved to be sufficient, but iterations might become necessary for data sets with higher water surface height fluctuations.

The described workflow was implemented and tested based on the scientific laser scanning software OPALS, but is entirely generic and can, thus, also be integrated into other software packages including LiDAR data processing software suites of laser scanner manufacturers.

References

Besl, P., McKay, N. D., 1992. A method for registration of 3-D shapes. *IEEE Transactions on Pattern Analysis and Machine Intelligence*, 14(2), 239-256.

Brun, A., Cucci, D. A., Skaloud, J., 2022. Lidar point–to–point correspondences for rigorous registration of kinematic scanning in dynamic networks. *ISPRS Journal of Photogrammetry and Remote Sensing*, 189, 185-200.

Fuchs, E., Tuell, G., 2010. Conceptual design of the CZMIL data acquisition system (DAS): integrating a new bathymetric lidar with a commercial spectrometer and metric camera for coastal mapping applications. *Algorithms and Technologies for Multispectral, Hyperspectral, and Ultraspectral Imagery XVI*, 7695(May 2010), 76950U.

Glira, P., Pfeifer, N., Briese, C., Ressl, C., 2015. A Correspondence Framework for ALS Strip Adjustments based on Variants of the ICP Algorithm. *PFG Photogrammetrie, Fernerkundung, Geoinformation*, 2015(4), 275–289. http://dx.doi.org/10.1127/pfg/2015/0270.

Glira, P., Pfeifer, N., Mandlburger, G., 2016. Rigorous Strip Adjustment of UAV-based Laserscanning Data Including Time-Dependent Correction of Trajectory Errors. *Photogrammetric Engineering & Remote Sensing*, 82(12), 945–954.

Guenther, G., 1985. Airborne laser hydrography: System design and performance factors. *NOAA Professional Paper Series*.

Guenther, G., Cunningham, A., Laroque, P., Reid, D., 2000. Meeting the accuracy challenge in airborne lidar bathymetry. *Proceedings of the 20th EARSeL Symposium: Workshop on Lidar Remote Sensing of Land and Sea*, Dresden, Germany.

Hickman, G. D., Hogg, J. E., 1969. Application of an airborne pulsed laser for near shore bathymetric measurements. *Remote Sensing of Environment*, 1(1), 47–58. http://www.sciencedirect.com/science/article/pii/S0034425769900881.

Jonassen, V. O., Kjørsvik, N. S., Gjevestad, J. G. O., 2023. Scalable hybrid adjustment of images and LiDAR point clouds. *ISPRS Journal of Photogrammetry and Remote Sensing*, 202, 652-662. https://www.sciencedirect.com/science/article/pii/S0924271623001880.

Kinzel, P. J., Legleiter, C. J., 2019. sUAS-Based Remote Sensing of River Discharge Using Thermal Particle Image Velocimetry and Bathymetric Lidar. *Remote Sensing*, 11(19). https://www.mdpi.com/2072-4292/11/19/2317.

Mandlburger, G., Pfennigbauer, M., Schwarz, R., Flöry, S., Nussbaumer, L., 2020. Concept and Performance Evaluation of a Novel UAV-Borne Topo-Bathymetric LiDAR Sensor. *Remote Sensing*, 12(6), 986. https://www.mdpi.com/2072-4292/12/6/986.

Otepka, J., Mandlburger, G., Karel, W., 2012. The OPALS data manager; efficient data management for processing large airborne laser scanning projects. *ISPRS Annals of the Photogrammetry, Remote Sensing and Spatial Information Sciences*, 1.

Pfeifer, N., Mandlburger, G., Otepka, J., Karel, W., 2014. OPALS –- A framework for Airborne Laser Scanning data analysis. *Computers, Environment and Urban Systems*, 45, 125–136.

Pfennigbauer, M., Ullrich, A., Steinbacher, F., Aufleger, M., 2011. High-resolution hydrographic airborne laser scanner for surveying inland waters and shallow coastal zones. *Proc. SPIE*, 8037, 803706–803711.

Pöppl, F., Ullrich, A., Mandlburger, G., Pfeifer, N., 2024. A flexible trajectory estimation methodology for kinematic laser scanning. *ISPRS Journal of Photogrammetry and Remote Sensing*, 215, 62-79.

Ressl, C., Kager, H., Mandlburger, G., 2008. Quality checking of als projects using statistics of strip differences. *IAPRS XXXVII*, 253–260.

Riegl, 2025. Data sheet of VQ-840-GE topographic and bathymetric full waveform scanner. https://www.riegl.com/en-austria/products/detail/riegl-vq-840-ge (2026-03-22).

Schwarz, R. K., Pfeifer, N., Pfennigbauer, M., Mandlburger, G., 2021. Depth Measurement Bias in Pulsed Airborne Laser Hydrography Induced by Chromatic Dispersion. *IEEE Geoscience and Remote Sensing Letters*, 18(8), 1332-1336.

Schwarz, R., Mandlburger, G., Pfennigbauer, M., Pfeifer, N., 2019. Design and evaluation of a full-wave surface and bottom-detection algorithm for LiDAR bathymetry of very shallow waters. *ISPRS Journal of Photogrammetry and Remote Sensing*, 150.

Szafarczyk, A., Toś, C., 2023. The Use of Green Laser in LiDAR Bathymetry: State of the Art and Recent Advancements. *Sensors*, 23(1). https://www.mdpi.com/1424-8220/23/1/292.

TU Wien, 2026. Official website of the scientific laser scanning software OPALS. https://opals.geo.tuwien.ac.at (2026-03-20).

Wozencraft, J. M., Lillycrop, W. J., 2003. SHOALS Airborne Coastal Mapping: Past, Present, and Future. *Journal of Coastal Research*, 38(SPEC. ISS), 207–215.